DESIGN AND ANALYSIS OF THE TRANSMISSION MECHANISM OF THE SERVO PRECISION PRESS FOR THE EXPLOSION PROOF VALVE OF THE NEW ENERGY BATTERY COVER

Yanzhong HE[1], Xingsong WANG[2]*, Chunlei TU[3]

The explosion-proof valve of new energy battery is closely related to the safety of new energy vehicles. As a result, the stamping process of explosion-proof valves and explosion-proof marks imposes a very high demand on the stamping accuracy and bottom dead center consistency of the press machine. Based on these special stamping process requirements, this paper proposes a new circular disk connecting rod main transmission mechanism. Compared with the traditional crank connecting rod mechanism, this transmission mechanism has fewer connecting parts that generate gaps, reducing the comprehensive clearance by 60%. This greatly improves the repeatability and positioning accuracy of the bottom dead center, and the lower transmission center of gravity makes it run at high speed more smoothly and reliably. In addition, combined with the closed-loop feedback control function of bottom dead point detection in the servo control system, the stamping accuracy of the servo precision press is further optimized and improved. This paper starts with the working principle of the mechanism, establishes the parametric model of the mechanism, and conducts Kinematics and dynamic analysis of the transmission mechanism. And the mechanism was simulated and verified using ADAMS software, providing a reference for the design of such servo precision presses.

Keywords: new energy, explosion-proof valve, circular disk connecting rod, servo, precision press machine, precision

1. Introduction

With the widespread promotion of new energy vehicles, the production capacity demand for core components such as new energy power batteries is also rapidly increasing year by year, from 160Gwh last year to 1800Gwh by 2025. With the rise of localization in the new energy vehicle industry chain, the demand

[1] Department of Mechanical Engineering Southeast University Nanjing, Jiangsu Province, China, 18136819996@163.com
[2] Department of Mechanical Engineering Southeast University Nanjing, Jiangsu Province, China, 642833654@qq.com
[3] Department of Mechanical Engineering Southeast University Nanjing, Jiangsu Province, China, hailingmm123@163.com

for stamping specialized machines for new energy power battery shells, covers, and explosion-proof valves in China will surge in the future[1-3].

The explosion-proof valve is a key component for the safe pressure relief of new energy power batteries. Its quality stability directly determines the safety of new energy vehicles and batteries. The burst value of the explosion-proof valve must be controlled within a certain tolerance range to ensure stable and reliable burst pressure, such as 0.8~0.9Mpa. The stability and consistency of the bursting pressure depend on the tolerance value of the stamping residual thickness of the explosion-proof valve disc. The smaller the tolerance value, the higher the bottom dead center repetition precision of the machine tool, and the stamping precision of the explosion-proof valve generally requires within 0.01mm[4-6].

Taking the 250 ton press machine as an example, the total deformation of the existing machine tool is about 0.5mm, the comprehensive clearance of the connecting part is 1.03mm, and the repeated positioning accuracy of the bottom dead center of the slider is ±0.2mm[7]. The above data indicators simply cannot meet the accuracy requirements of the explosion-proof valve plate stamping. However, imported precision presses from abroad are not only expensive but also have a long delivery time, far from meeting the development needs of such special stamping processes in China. Therefore, the development of an explosion-proof valve plate stamping machine with extremely high precision for stamping and repetitive positioning is of strategic significance for the development of new energy.

The servo precision press proposed in this article, due to the use of a low comprehensive clearance disc connecting rod transmission mechanism, combined with a servo closed-loop control system, can achieve the requirement of explosion-proof valve stamping accuracy within 0.01mm, filling the equipment gap of domestic explosion-proof valve stamping special machines.

2. The proposal of the main transmission mechanism for servo precision press machines

Based on the above process requirements, a new type of main transmission mechanism for the press has been proposed.Fig.1 shows the schematic diagram of the main transmission mechanism for the press machine. In the Fig.1 represents the guide rail 2 represents the slide 3 represents the circular disk connecting rod, and 4 represents the crankshaft. The slide is installed inside the guide rail, and the circular disk connecting rod is connected to the center position of the slide, while the crankshaft is connected to the eccentric position of the circular disk connecting rod [8].

The crankshaft rotates in a clockwise direction as indicated by the arrow, and when the center axis of the slide's vertical movement is located to the right of

the crankshaft's rotation center axis, it is referred to as a positive offset, whereas it is a negative offset when located to the left. The bottom dead center of this mechanism is achieved when the circular disk connecting rod overlaps with the crankshaft, and the distance from the crankshaft center to the slide center is obtained by subtracting the crankshaft length from the connecting rod length, hence termed as the subtractive method. In contrast, the bottom dead center of traditional press machines is reached when the crankshaft and connecting rod are in line, and the distance from the crankshaft center to the slide center is obtained by adding the crankshaft length and connecting rod length, thus termed as the additive method. This paper adopts the positive offset subtractive method crank-slider mechanism [9].

The working principle of this mechanism is that when the crankshaft rotates, it drives the circular disk connecting rod to rotate inside the slide, which, in turn, drives the slide to move up and down along the centerline of its motion. By designing different geometric parameters while satisfying the required relationships among them, different motion curves of the slide can be obtained, which correspond to different process characteristics of the slide. By reasonably changing the corresponding geometric parameters, the speed of the slide at the end of the working stroke can be greatly reduced, and the mechanism can maintain pressure near the bottom dead center for a certain period of time, thereby endowing the mechanism with the process characteristic of stretching and holding pressure.

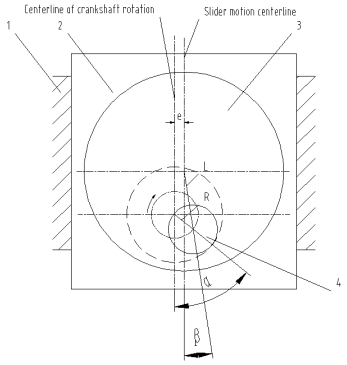

Fig. 1 Schematic diagram of the new transmission mechanism

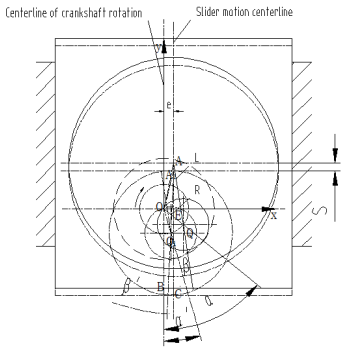

Fig. 2 Simplified diagram of the parameterization of the new transmission mechanism

1. Guide rail, 2. slide, 3. circular disk connecting rod, 4. crankshaft.

3. Kinematic analysis of the new transmission mechanism

3.1 Establishment of a parameterized structural model for the transmission mechanism

Fig.2 shows a simplified parameterized diagram of the new transmission mechanism for a press. The coordinate system is established with the crankshaft

rotation center O as the origin, the horizontal direction as the x-axis, and the vertical direction as the y-axis. The rotation center of the circular disk connecting rod is at point A, the eccentric neck center of the crankshaft is at point Q, the intersection of the crankshaft's vertical centerline with the slide's bottom edge is at point B, the intersection of the slide's vertical motion centerline with the bottom edge is at point C, the intersection of the slide's vertical motion centerline with the x-axis is at point E, an arbitrary point on the eccentric neck center of the crankshaft is at point Q_1, and the center of the circular disk can be located at any position denoted by A'. The operating principle is that as point Q rotates around point O, the circular disk connecting rod rotates around its center A inside the slide, while point A rotates around the center of the crankshaft, causing the slide to move up and down within the guide rail [10]. In the Fig., $OQ = R$ is the crank radius, $AQ = L$ is the length of the circular disk connecting rod, i.e., the distance between the eccentric hole on the circular disk and its center point A, and the distance between the centerline of the slide with positive (right) offset from the crankshaft centerline is $OE = e$. R, L, e are all constant values. The angle between the crankshaft and the vertical direction is denoted by $\angle QOB = \alpha$, and the angle between the circular disk connecting rod $AQ = L$ and the vertical motion line of the slide is denoted by $\angle QAC = \beta$.

3.2 Analysis of the motion characteristics of the transmission mechanism

Kinematic analysis of a transmission system refers to analyzing the output motion law of the slide based on the known geometric parameters and motion characteristics of the transmission mechanism.

Given the geometric parameters as shown in Fig.2, including the crank radius R, the length of the circular disk connecting rod L, and the displacement distance e between the slide's motion centerline and the crankshaft rotation centerline.The proportional relationship among them is denoted by $\lambda = R/L$, $K = e/R$, $\lambda K = e/L = \varepsilon$. When the crankshaft rotates from Q to Q_1, the crankshaft rotation angle is denoted by $\angle Q_1OB = \alpha'$, and the angle between the circular disk connecting rod AQ and the slide's motion centerline is denoted by $\angle Q_1A_1C = \beta'$, where $OQ = OQ_1 = R$ and $AQ = A_1Q_1 = L$. The displacement of the slide is given by the vertical coordinate $y = AE$ of point A, therefore, $Y_A - Y_{A_1}$ denotes the travel distance of the slide, i.e. $S = Y_A$.

(1)Displacement of the slide

According to the geometric relationship shown in Fig.2, the displacement

angle relationship of the slide is given by the following equation:

$$S = Y_A = L\cos\beta - R\cos\alpha = L\sqrt{1-\left(\frac{R\sin\alpha - e}{L}\right)^2} - R\cos\alpha \tag{1}$$

Substituting $\lambda = R/L$, $K = e/R$ and $\lambda K = e/L = \varepsilon$ into Eq.(1), the displacement equation is obtained as follows:

$$S = L\sqrt{1-(\lambda\sin\alpha - \varepsilon)^2} - R\cos\alpha \tag{2}$$

If the crank radius R, the length of the circular disk connecting rod (eccentric hole distance) L, and the positive offset distance e of the crank-slider mechanism are given, the relationship curve between the slide displacement S and the crankshaft rotation angle α can be obtained according to Eq.(2) [11-14].

(2)The velocity of the slide

Solving Eq.(2), the relationship between the slide velocity v and the crankshaft rotation angle α is given by:

$$v = \omega\frac{d}{d\alpha}\left[L\sqrt{1-(\lambda\sin\alpha - \varepsilon)^2} - R\cos\alpha\right] \tag{3}$$

(3)Slide acceleration

Solving Eq.(3), we obtain the expression for the crankshaft rotation angle a as:

$$a = \frac{d}{d\alpha}\left\{\omega^2\frac{d}{d\alpha}\left[L\sqrt{1-(\lambda\sin\alpha - \varepsilon)^2} - R\cos\alpha\right]\right\} \tag{4}$$

4. Analysis of mechanical characteristics of the transmission mechanism

The positive-offset subtraction formula crank-slider mechanism is mainly composed of a crankshaft, a circular disk connecting rod, and a slide, and its force state is mainly analyzed in terms of the crankshaft carrying capacity, torque, and the force on the circular disk connecting rod.

4.1 Crankshaft torque

The torque M_e applied to the crankshaft includes the load torque M_F and the friction torque M_μ of the crank-slider transmission mechanism, i.e.,

$$M_e = M_F + M\mu \tag{5}$$

(1) Load torque.

Under the action of the nominal force P_n applied on the slide, the load torque borne by the crankshaft can be derived as follows:

$$M_F = P_n R\sin\beta(1/\sin\varphi) \tag{6}$$

Where, φ denotes the transmission angle where the nominal force occurs, i.e.,

$$\cos\varphi = (R\sin\alpha \pm e)/L \tag{7}$$

In a direct-offset crank-slider mechanism, $e=0$, while in a negative-offset mechanism, e is denoted by a "+" sign, and in a positive-offset mechanism, e is denoted by a "-" sign. Under the same conditions of R、L、e, $\cos\varphi$ is minimum for a positive offset, i.e., φ is maximum. Therefore, in Eq.(6), it can be observed that φ is maximum, $\sin\varphi$ is also maximum, and hence M_F is minimum. Therefore, the transmission mechanism designed in this paper has the beneficial effect of reducing torque under the same load conditions.

(2) Friction torque

T Friction is an inevitable phenomenon between any two moving components, which results in the generation of frictional resistance torque in a system. In the crank-slider mechanism as shown in Fig.3, the sources of friction include the sliding contact between the slide and the guide surface of the body, the bearing contact between the two support necks of the crankshaft and the bearings, the contact between the crankshaft neck and the circular disk connecting rod, and the contact between the circular disk connecting rod and the large copper bushing. The friction torque of each friction source is calculated separately as follows[15, 16].

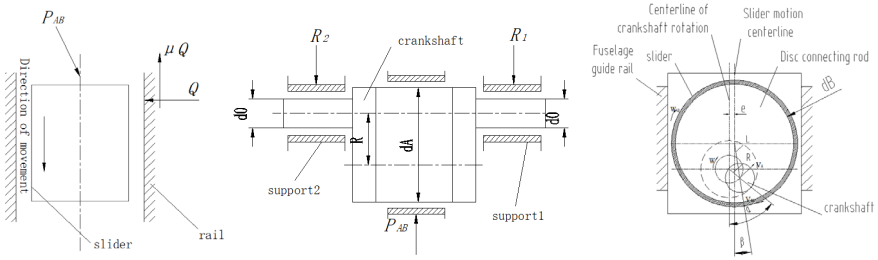

a) b) c)

Fig. 3 Friction sources in the crank-slider transmission mechanism

1) Friction between the slide and the guide surface of the body is shown in Fig. 3a, and the frictional force here is denoted by P_μ.

$$P_\mu = \mu Q = \mu P\lambda\sin\alpha \tag{8}$$

Where, μ is the coefficient of friction, Q is the reactive force of the guide on the slide, and λ is the link coefficient.

Applying the power balance principle, the frictional force P_μ can be converted into an equivalent friction torque M_1 on the crankshaft, i.e.,

$$M_1\omega = P_\mu v \tag{9}$$

Substituting the slide velocity v from Eq.(3) and the frictional force P_μ

from Eq.(8) into the above equation yields:

$$M_1\omega = P_\mu v = \mu P\lambda \sin\alpha * \omega \frac{d}{d\alpha}\left[L\sqrt{1-(\lambda\sin\alpha-\lambda K)^2} - R\cos\alpha\right] \tag{10}$$

After rearrangement, we have：

$$M_1 = \mu P\lambda \sin\alpha \frac{d}{d\alpha}\left[L\sqrt{1-(\lambda\sin\alpha-\lambda K)^2} - R\cos\alpha\right] \tag{11}$$

2) Friction between the two support necks of the crankshaft and the bearings is shown in Fig.3b. The frictional force is distributed on the working surface of the crankshaft support necks and the friction torque acting on the crankshaft is denoted by M_2.

$$M_2 = \mu\ （R_1 + R_2）\frac{d_0}{2} = \mu P\frac{d_0}{2} \tag{12}$$

$\left(F_{R_1} + F_{R_2}\right) = P_{AB} = P_g$.Where, d_0 is the diameter of the crankshaft support necks, F_{R_1}、F_{R_2} are the reactive forces acting on support 1 and support 2, respectively, and it is assumed that $\left(F_{R_1} + F_{R_2}\right) = P_{AB} = P_g$.

3) Friction between the crankshaft neck and the circular disk connecting rod bearing is shown in Fig.3b. The frictional force here is distributed on the cylindrical surface of the crankshaft neck, and the resistance torque borne by the crankshaft neck is denoted by m.

$$M_A = \mu P_{AB}\frac{d_A}{2} = \mu P_g\frac{d_A}{2} \tag{13}$$

Where, d_A is the diameter of the crankshaft neck.

Similarly, based on the power balance principle, the resistance torque M_A can be converted into an equivalent friction torque M_3 on the crankshaft, i.e.,

$$M_3\omega = M_A(\omega + \omega_{AB}) \tag{14}$$

Where, ω_{AB} is the angular velocity of the circular disk connecting rod, as shown in Fig.3c, which can be calculated from the following equation:

$$\omega_{AB} = v_{BA} / L \tag{15}$$

Where, v_{BA} is the relative velocity of the circular disk connecting rod, which can be obtained from the velocity triangle in Fig. 3c, i.e.,

$$v_{BA} = v_A\frac{\sin(90^o-\alpha)}{\sin(90^o-\beta)} = -v_A\frac{\cos\alpha}{\cos\beta} = -R\omega\frac{\cos\alpha}{\cos\beta} \tag{16}$$

Then we have

$$\omega_{AB} = -\frac{R}{L}\omega\frac{\cos\alpha}{\cos\beta} = -\lambda\omega\frac{\cos\alpha}{\cos\beta} \tag{17}$$

Considering $\cos\beta \approx 1$, the above equation can be simplified as:

$$\omega_{AB} = -\lambda\omega\cos\alpha \tag{18}$$

Substituting M_A and ω_{AB} into Eq.(14) and simplifying, we have:

$$M_3 = \frac{1}{2}(1-\lambda\cos\alpha)\mu d_A P \tag{19}$$

4) Friction between the circular disk connecting rod and the slide is shown in Fig. 3c, and the resistance torque M_B can be calculated as follows:

$$M_B = \mu P_{AB}\frac{d_B}{2} = \mu P\frac{d_B}{2} \tag{20}$$

Where d_B is the outer diameter of the circular disk connecting rod. The resistance torque M_B can be converted into an equivalent friction torque M_4 on the crankshaft as follows:

$$M_4 = -\frac{1}{2}d_B\mu\lambda P_g\cos\alpha \tag{21}$$

Therefore, the total friction torque acting on the crankshaft M_μ is given as follows:

$$M_\mu = M_1 + M_2 + M_3 + M_4 \tag{22}$$

Substituting Eq.(11), (12), (19), and (21) into Eq.(22) and simplifying, we get:

$$M_\mu = \frac{1}{2}\mu P\left[2\lambda R\sin\alpha\left(\sin\alpha - \frac{\lambda}{2}\sin 2\alpha\right) + d_0 + (1-\lambda\cos\alpha)d_A - \lambda d_B\cos\alpha\right] \tag{23}$$

As seen from the above equation, the friction torque M_μ acting on the crankshaft varies with the crank angle α.

4.2 Lateral force on the slide

According to Fig.3a and Fig.3c, the lateral force F_{HC} on the slide can be derived as:

$$F_{HC} = P_{AB}\times\sin\beta \tag{24}$$

Since the angle β is very small, then we have $\cos\beta \approx 1$, and considering $P_{AB} = P_n$

Therefore, Eq.(24) can be rewritten as:

$$F_{HC} = P_d(R\sin\alpha \pm e)/L \tag{25}$$

In a straight-slider crank mechanism, e=0, a negative offset e is denoted by "+", and a positive offset e is denoted by "-". It is obvious that among the three mechanisms, the lateral force on the slide is the smallest when the slider has a positive offset.

5. Optimization design of transmission system mechanisms

Optimization design of transmission system mechanisms is a type of

multi-variable, multi-constraint, non-linear optimization problem. In this paper, genetic algorithm is used to optimize the design of the transmission system of a press machine.

Due to the fact that the punching force of this type of press mainly relies on the instantaneous peak torque of the servo motor to provide power, it is required that the instantaneous peak torque of the servo motor be relatively large. In order to reduce the demand for peak torque of the motor by the transmission mechanism, optimizing the size of the transmission mechanism to minimize the peak torque required by the motor is an important goal. In addition, in order to meet the stretching process requirements of the press, the running speed of the slider during the stamping stage gradually slows down and pressurizes, and even the bottom dead center stays and maintains pressure, which is also a key indicator to be considered during mechanism design [17-20]. Therefore, in order to achieve the optimal motion and force characteristics of the transmission mechanism, it is very important to design the optimal key rod length parameters of the transmission mechanism.

The key parameters of the main transmission mechanism mainly include the crank radius R, the length of the circular disk connecting rod L, the offset distance between the slide running centerline and the crankshaft rotation centerline e, the outer diameter of the circular disk d_B, and the inner diameter of the eccentric hole d_A.

5.1 Establishing an optimization design model.

Genetic algorithm is applied to optimize the key parameters of the mechanism.

(1) Determining parameter variables: The five parameters R, L, e, d_B, d_A are selected as the independent variables for the optimization design of the circular disk connecting rod transmission mechanism.

$$X = [R, L, e, d_B, d_A]^T \tag{26}$$

(2) Determining the objective function: The objective function $f(X)$ is defined as follows:

$$\min f(X) = \alpha M_F + (1-\alpha)\Delta\nu \tag{27}$$

Where α is the weighting coefficient, which takes a value within the range of $[0,1]$, M_F is the nominal torque acting on the crankshaft, $\Delta\nu$ is the velocity fluctuation value of the slide near the nominal pressure stroke S_g. The velocity fluctuation value $\Delta\nu$ in this range is calculated using the following equation:

$$\Delta\nu = \frac{1}{n}\sum_{i=1}^{n}\left|\nu_i - \bar{\nu}\right| \tag{28}$$

5.2 The optimization design results and analysis

Assuming the rated load acting on the circular disk connecting rod mechanism is $P_n = 2500kN$, the nominal pressure stroke is $S_g = 2mm$, the slide stroke is $S = 100 \pm 1mm$, and the number of stroke cycles is $N_n = 60spm$. The values of the parameter variables are shown in Table 1. Similarly, the minimum torque and minimum velocity fluctuation in the given area $\lfloor S_g - 0.2, S_g + 0.2 \rfloor$ at the nominal pressure stroke $S_g = 2mm$ are set as the dual optimization objectives, with equal weights [21].

Table 1

Range of values for parameter variables of the circular disk connecting rod mechanism

	R [mm]	L [mm]	e [mm]	d_B [mm]	d_A [mm]
Lower limit	49	50	0	650	450
Upper limit	51	80	20	800	600

Running the genetic algorithm optimization design program for the circular disk connecting rod mechanism, the optimization design results were obtained after 150 generations of genetic evolution, as shown in the calculation results presented in Table 2.

Genetic parameter statistics:

Total number of crossover operations = 7958, total number of mutation operations = 4515, number of unsuccessful crossovers = 0, number of unsuccessful mutations = 5.

Table 2

Calculation results of genetic algorithm optimization for circular disk connecting rod mechanism

----------after 150 generations of genetic evolution ----------										
	R [mm]	L [mm]	e [mm]	d_B [mm]	d_A [mm]	M_F [Nm]	F_{HC1} [N]	F_{HC2} [N]	t_b [s]	Fitness [mm]
1)	50	70	0	750	520	20619	937326	0	0.206	0.937109
2)	50	75	0	750	530	21800	807256	0	0.193	0.936231
3)	50	80	0	750	535	22796	712137	0	0.191	0.936003
……										
115)	50	70	4	750	520	19409	-435703	510310	0.085	0.923023
116)	50	70	8	750	520	18535	-72038	1091089	0.085	0.923023
117)	50	70	10	750	520	18216	-351079	1443375	0.084	0.872971

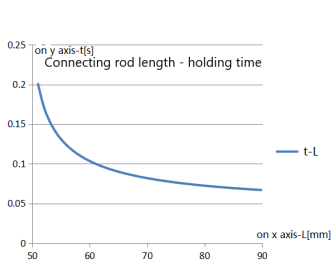

a) the relationship curve between connecting rod length and holding pressure time

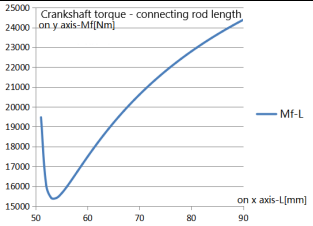

b) the relationship curve between crankshaft torque and connecting rod length

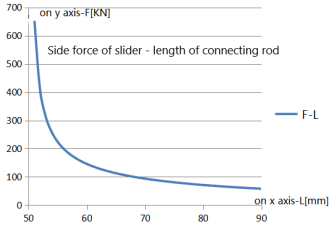

c) the relationship curve between lateral force and connecting rod length

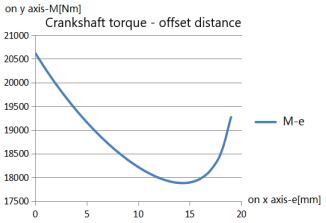

d) the relationship curve between crankshaft torque and offset distance

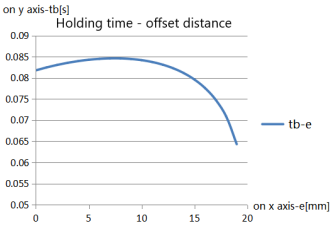

e) the relationship curve between holding pressure time and offset distance

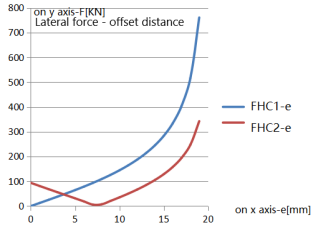

f) the relationship curve between lateral force and offset distance

Fig.4 The relationship between connecting rod length, torque, time, force, and distance

Minimum fitness: 0.8575363, maximum fitness: 0.9371092, average fitness: 0.9027657.

The best individual found so far => Generation: 137.

Based on data analysis, the following correlation tables were obtained. Fig.4a shows the relationship curve between connecting rod length L and holding pressure time t_b. Fig.4b shows the relationship curve between crankshaft torque M_F and connecting rod length L. Fig.4c shows the relationship curve between lateral force F_{HC1} at the nominal force stroke of the slide and connecting rod length L. Fig.4d shows the relationship curve between crankshaft torque M_F and offset distance e. Fig.4e shows the relationship curve between pressure holding time t_b and offset distance e. Fig.4f shows the relationship curve between lateral forces F_{HC1} and F_{HC2} of the slide and offset distance e [22].

Based on the above relationship curves, it can be inferred that: As shown in Fig.4a, the longer the connecting rod length, the shorter the holding pressure time. As shown in Fig.4b, when the offset distance $R = 50mm$ is present, there is a turning point in the relationship between the connecting rod length and crankshaft torque at $L = 53.5mm$, when $L\langle 53.5mm$, the larger the connecting rod length, the smaller the crankshaft torque. After $L\rangle 53.5mm$, the larger the connecting rod length, the larger the crankshaft torque, indicating a positive correlation between

crankshaft torque and connecting rod length. As shown in Fig.4c, the changing trend of the relationship between lateral force F_{HC1} and connecting rod length L occurs at $L = 58mm$. When $L\langle 58mm$, the larger the connecting rod length, the more rapid the decrease in lateral force F_{HC1}. After $L\rangle 58mm$, the larger the connecting rod length, the more gradual the decrease in lateral force F_{HC1}. As shown in Fig.4d, there is a turning point in the relationship between crankshaft torque M_F and offset distance e at $e = 15mm$. When $e\langle 15mm$, the larger the offset distance e, the smaller the crankshaft torque. After $e\rangle 15mm$, the larger the offset distance, the larger the crankshaft torque. As shown in Fig.4e, there is a turning point in the relationship between holding pressure time t_b and offset distance e at $e = 8mm$. When $e\langle 8mm$, the larger the offset distance, the slower the increase in holding pressure time. After $e\rangle 8mm$, the larger the offset distance, the more rapid the decrease in holding pressure time. As shown in Fig.4f, the relationship between lateral force F_{HC1} at the nominal force stroke of the slide and offset distance e is that the larger the offset distance e, the larger the lateral force F_{HC1}. However, the relationship between lateral force F_{HC2} of the slide at the bottom dead center and offset distance e has a turning point at $e = 7mm$. When $e\langle 7mm$, the larger the offset distance e, the smaller the lateral force F_{HC2}. After $e\rangle 7mm$, the larger the offset distance, the larger the lateral force F_{HC2} of the slide.

Based on the above analysis, the following two sets of data are considered the best, as shown in Table 3:

Table 3

Two sets of optimal parameters for the disc connecting rod mechanism

	R [mm]	L [mm]	e [mm]	d_B [mm]	d_A [mm]	M_F [Nm]	F_{HC1} [N]	F_{HC2} [N]	t_b [s]	Fitness [mm]
1	50	70	0	750	520	20619	937326	0	0.206	0.937109
2	50	70	4	750	520	19409	-435703	510310	0.085	0.923023

As shown in Fig.5, the relationship curve between slide stroke and time for Data 1 demonstrates a clear holding motion characteristic, which is suitable for the process requirements of servo presses and can meet the process needs for holding pressure in both forward and reverse directions. Fig.6 shows the lateral force curve for Data 1, from which it can be seen that the lateral force of the slide gradually decreases to zero as it approaches the bottom dead center, and the maximum lateral force at the nominal force stroke position is around 93 tons. Fig.7 shows the relationship curve between slide stroke and time for Data 2, which exhibits a distinct rapid return characteristic with low-speed stamping, and

a slightly shorter holding time. Fig.8 shows the lateral force curve for Data 2, from which the lateral force of the slide reverses near the bottom dead center. Therefore, during rapid stamping, the lateral force will generate alternating loads on both sides of the guide rail, which is detrimental to maintaining the precision of the slide guide rail. Although this design scheme has smaller crankshaft torque and maximum lateral force of the slide, it is not suitable due to the reversal of the lateral force near the bottom dead center.

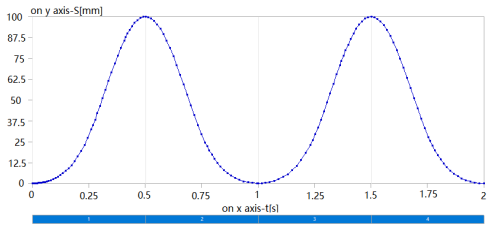

Fig.5: Slide stroke-time curve for Data 1

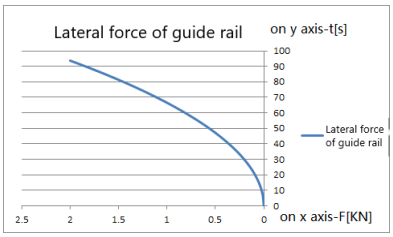

Fig.6: Lateral force curve for Data 1

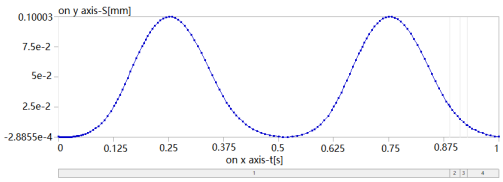

Fig.7: Slide stroke-time curve for Data 2

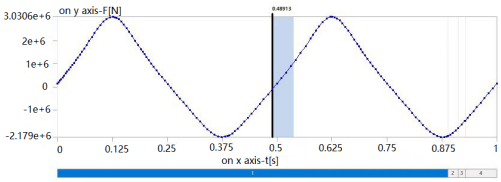

Fig.8: Lateral force curve for Data 2

Based on the above data analysis, the optimal variable parameters for the selected individual are shown in Table 4:

Fig.9 shows the final optimized slide displacement curve for the disc connecting rod mechanism, which exhibits a relatively smooth motion near the bottom dead center and a significant holding characteristic. The motion curve is very ideal.

Table 4

Optimal design results of variable parameters for the disc connecting rod mechanism

	R [mm]	L [mm]	e [mm]	d_B [mm]	d_A [mm]	M_F [Nm]	F_{HC1} [KN]	F_{HC2} [KN]	t_b [s]	Fitness [mm]
1	50	70	0	750	520	20619	937326	0	0.206	0.937109

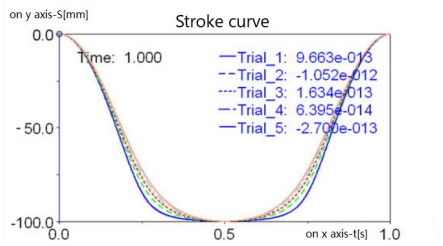

Fig.9: Optimized slide displacement curve

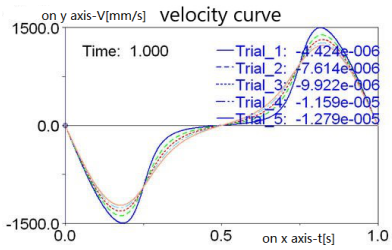

Fig.10: Optimized slide velocity curve

Fig.10 shows the final optimized slide velocity curve, from which the

velocity changes smoothly from 160 to 200 degrees near the bottom dead center, indicating good low-speed control.

6. Simulation analysis and verification of the main transmission mechanism

Dynamic simulation experiments were conducted on the created transmission system model using the ADAMS/View functional module. The simulation results were displayed in the form of curve graphs using the ADAMS/Post Processor functional module, to analyze the simulation results.

For the convenience of calculation, the number of slider strokes is set according to N=60spm. Rolling bearings are used for the front and rear bearings of the crankshaft and the journal bearings of the crankshaft. Due to the small clearance, it can be ignored. The eccentric wheel and slider use sliding bearings, and the clearance is set according to $\varsigma = \frac{d_B}{7000} = 0.107mm$. Based on the above boundary conditions and key technical indicator parameters, the driving control function was set as shown in Table 5 [23, 24].

Table 5

Control function for simulating the slide motion curve of the ADAMS virtual prototype.

No.	Curve Mode	Control function
1	Multi-linkage mode	step(MOD(time, 1), 0, 0d, 0.3, 120d)+step(MOD(time, 1), 0.15, 0d, 0.65, 60d)+step(MOD(time, 1), 0.6, 0d, 0.68, 0d)+step(MOD time, 1), 0.65, 0d, 1, 180d)
2	Pendulum mode	step(MOD(time, 1), 0, 160d, 0.5, 200d)+step(MOD(time, 1), 0.5, 0d, 1, -160d)

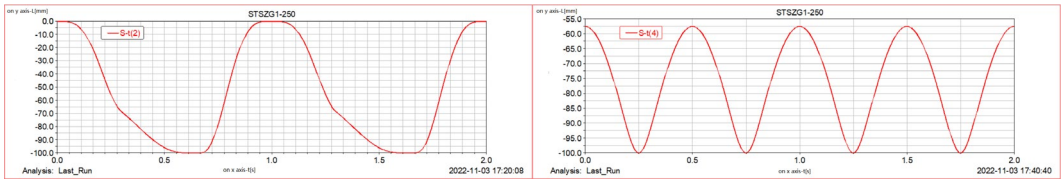

(a)multi-linkage mode (b)Pendulum mode

Fig. 11: Simulation curve of the slide motion for the virtual prototype

By using the control function in Table5 for simulation of the virtual prototype, the motion curves for each mode can be obtained, as shown in Fig.11(a) Multi-linkage mode, which controls the speed during the slide motion to simulate the characteristics of low-speed stamping and fast return of the slide, which is better than that of mechanical multi-linkage machine tools. As shown in the curve, the slide speed is reduced by 80% when the crankshaft rotation angle is 120° (37mm height above bottom dead center) to adapt to the stretching speed of the

material, and then the slide speed is increased by 100% for fast return after passing through the bottom dead center of 180°. Fig.11(b) Pendulum mode, which is used for rapid blanking or progressive die processing to improve production efficiency. The slide moves back and forth at a suitable position away from the bottom dead center for stamping processing, as shown in the curve, where the slide moves back and forth for processing when the crankshaft rotation angle is 120° (37mm height above bottom dead center).

Based on the above simulation curves, it can be concluded that the various modes of slide motion are all in line with the design requirements. Therefore, the design parameters of the prototype are reasonable and in line with the expected design.

7. Servo precision press closed-loop control scheme

To improve the accuracy of repeated positioning of the bottom dead center of the precision press, not only should the comprehensive clearance be reduced from the mechanical structure, but also the closed-loop feedback compensation control of the slider's movement should be achieved from the control system, further improving the accuracy of repeated positioning of the slider at the bottom dead center. Through closed-loop control, accuracy issues caused by equipment deformation can be avoided, such as dead spot blind spots, rigid micro deformation, and structural micro deformation caused by environmental temperature.

The closed-loop control scheme is: fast down - deceleration - micro speed - suppression stop - micro speed return - fast return. The displacement sensor body used in this scheme is separated from the contact, reducing frictional resistance and achieving high accuracy. And the displacement sensor adopts a micrometer level accuracy of 0.002mm as position feedback, and adopts Ethercat communication, which has fast communication speed and high control response.

In addition, as shown in Figure 18, Ethercat communication is adopted, which means that the first Ethernet communication interface circuit uses an industrial Ethernet interface, and the second Ethernet communication interface circuit uses a real-time Ethernet interface that supports the EtherCAT master station protocol stack. This not only has fast communication speed, but also high control response.

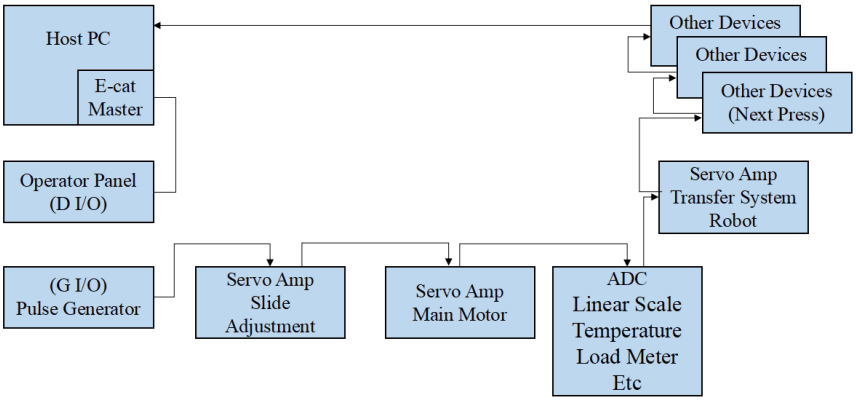

Fig.12:E-CAT Electrical Control Composition Diagram

8. Conclusion

Through the design and analysis of the new disc-linkage main transmission mechanism for the servo precision press in this paper, it is found that the application of the eccentric sleeve disc-linkage structure on the press can achieve a better slide stroke curve. Meanwhile, due to the reduction of the transmission center of gravity and the elimination of the unbalanced force generated by the linkage swing, the high-speed operation of the machine tool is more stable. The height of the machine body is reduced by at least 1/3 for the same tonnage machine, which further improves the stiffness of the machine body [25]. Due to the reduction of 2/3 in the areas that generate clearance compared to traditional structures, and the use of rolling bearings instead of sliding bearings in heavy-duty impact areas, the comprehensive clearance is further reduced. The comprehensive clearance is more than 2/3 smaller than traditional machine tools, And the servo closed-loop control scheme is adopted to ensure the smooth and impactless transition point of the slider, which plays a positive role in ensuring accuracy. The precision of repeated positioning of the bottom dead center has been greatly improved, and the current controllable range of accuracy is within 0.005mm, which can achieve high-precision explosion-proof valve stamping and explosion-proof scoring processing.

In the future, the polynomial interpolation algorithm of the servo closed-loop control program can be optimized to make the slider motion curve of the press highly consistent with the required curve of the stamping process, which can further improve the stamping quality and accuracy, and better meet the requirements of the explosion-proof valve stamping process and precision stamping process.

REFERENCES

[1] Chinese Society for Mechanical Engineering, Forging Society. Handbook of Forging, Volume 3. Beijing: Machinery Industry Press, 1993.

[2] *He Deyu*. Special Purpose Press. Beijing: Machinery Industry Press, 1989.

[3] *H.Yanzhong*. "Research on Fuzzy Intelligent Control Algorithm for Servo Press". Forging & Stamping Equipment and Manufacturing Technology, **Vol. 55, No. 6.**

[4] *P.Kali, G.Aishwary, K.Hariharan,C.Uday,B.Dilip K., L.M.Gyu*. "Does friction contribute to formability improvement using servo press". Journal, Friction.**Vol.11, No. 5**. 2023.PP. 820-835.

[5] *G.Peter,B.Alexander,C.Kelin,M.Dirk A.,H.Jinjin,K.Brad L.,K.Yannis P.* "Effectiveness of different closed-loop control strategies for deep drawing on single-acting 3D Servo Presses".Journal,CIRP Annals -Manufacturing Technology.**Vol.71,No.1**.2022.PP .357-360.

[6] P.S M. "Robust optimization of a deep drawing process". Materials Science and Engineering. **Vol.1031, No.1**. 2021.PP .012007.

[7] *Z.Chenglin*. "Forging and Stamping Equipment". Xi'an: Northwestern Polytechnical University Press, 1987.

[8] Editorial Committee of Forging Technology Handbook. Forging Technology Handbook. Beijing: National Defense Industry Press, 1988.

[9] *R.Halicioglu,L.C.Dulger,A.T.Bozdana*."Structural design and analysis of a servo crank press".Engineering Science and Technology, an International Journal.**Vol.19**, **No.4**,2016,PP.2060-2072.

[10] *Z.Hongde, L.Hui*. "Table speed regulation function of mechanical press working area". Forging & Stamping Machinery, **Vol.5**, **No.4.**1997.PP.42-43.

[11]MCS. Software . MSC.ADAMS/View Advanced Training Course. Beijing: Tsinghua University Press,2004.

[12] *L.Yan, Z.Jianguo, R.Shu*. "Development and future trends of the latest servo presses". Forging&Stamping Equipment and Manufacturing Technology,**Vol.01**, **No.3**.2006.PP.11-14.

[13] S.*Kitayama, T.Higuchi,M.Takano, A.Kobayashi*. "Determination of back-pressure profile and slide motion of servo press in cold forging using sequential approximate optimization".Journal of Advanced Mechanical Design, Systems, and Manufacturing.**Vol.4**, **No.4**.2020.PP.0046-0049

[14] *S.Yousong, Zh.Xianhui, L.Mian, et al.* "AC servo press and its key technologies". Forging Technology, **Vol.33**, **No.4**.2008.PP.1-8.

[15] *Z.Anjun*. "Detection and analysis of stamping force, bottom dead center and vibration of servo press". Nanjing: Southeast University, 2008.

[16] *A.D.Prete;T.Primo*."Sheet Metal Forming Optimization Methodology for Servo Press Process Control Improvement". Journal, Metals.**Vol.10**,**No. 2**.2020. PP. 271-271.

[17] *F.Yan, Z.Liwei, D.Bo, et al."* New flexible forging technology - servo press". Metalworking (Hot Working), **Vol.15**.2009.PP.55-56.

[18] *F.Ya, S.Yousong, S.Guoliang, et al*. "Energy consumption analysis and energy-saving approaches of crank press". Forging Technology.**Vol.35**,**No.1.**2010.PP.110-113.

[19] *O.Nozomu; M.Luke; K.Hyunok; K.Alex*. "Profit-Driven Methodology for Servo Press Motion Selection under Material Variability". Journal, Applied Sciences. **Vol.11**, **No.20**. 2021. PP. 9530-9530.

[20] *B.Iker J, M.R.Fernando,M.Isidoro,H.Gregory G, M.I.Sergio*. "The influence of calculation method and relative strength on the load-velocity relationship in bench press exercise". Journal, International Journal of Sports Science & Coaching.**Vol.17**, **No. 3**. 2022.PP. 576-582.

[21] *Y.Chunsheng, H.Wenjie, Z.Junwei, et al.* "Research on digital servo press control system". Forging Technology,**Vol.34**,**No.6.** 2009.PP.117-122.

[22] K.*H.Sol,K.S.Il*. "Topology and Multi-Objective Structural Optimization of Frame Structure for a Mechanical Press with Capacity of 300 Ton". Journal of the Korean Society for Precision Engineering.**Vol.36, No.3**. 2019.PP. 247-253.

[23] *Z.Huixiong, Y.Chunsheng, M.Jianhua, et al*." Simulation study on servo press control system based on MATLAB". Forging Technology, **Vol.35, No.5.**2010.PP.69-75.

[24] L.Jianjun, R.Feng. "Design of digital control system for servo press. Forging Technology", **Vol.36, No.1.**2011. PP.93-97.

[25] *P.Cristian;D.Ioan;C.Romeo*. "The Influence of Ribbing of Mechanical Crank Press Cast C-Frames over the Stress State in Critical Areas". Journal, Applied Sciences.**Vol.12, No.11.**2022.PP. 5619-5619